STRUCTURAL BIOLOGY COMMUNICATIONS

ISSN 2053-230X

Structure of *Methylobacterium extorquens* malyl-CoA lyase: CoA-substrate binding correlates with domain shift

Javier M. González,‡ Ricardo Marti-Arbona,* Julian C.-H. Chen and Clifford J. Unkefer*

Bioscience Division, Los Alamos National Laboratory, Los Alamos, NM 87545, USA. *Correspondence e-mail: rm-a@lanl.gov, unkeferc@gmail.com

Received 14 December 2016
Accepted 19 January 2017

Edited by J. Newman, Bio21 Collaborative Crystallisation Centre, Australia

‡ Present address: Instituto de Bionanotecnología del NOA, Consejo Nacional de Investigaciones Científicas y Técnicas, Universidad Nacional de Santiago del Estero, G4206XCP Santiago del Estero, Argentina.

Keywords: biofuels; metabolic engineering; methanol; malyl-CoA lyase; *Methylobacterium extorquens*.

PDB reference: malyl-CoA lyase, 5ugr

Supporting information: this article has supporting information at journals.iucr.org/f

Malyl-CoA lyase (MCL) is an Mg^{2+}-dependent enzyme that catalyzes the reversible cleavage of (2*S*)-4-malyl-CoA to yield acetyl-CoA and glyoxylate. MCL enzymes, which are found in a variety of bacteria, are members of the citrate lyase-like family and are involved in the assimilation of one- and two-carbon compounds. Here, the 1.56 Å resolution X-ray crystal structure of MCL from *Methylobacterium extorquens* AM1 with bound Mg^{2+} is presented. Structural alignment with the closely related *Rhodobacter sphaeroides* malyl-CoA lyase complexed with Mg^{2+}, oxalate and CoA allows a detailed analysis of the domain motion of the enzyme caused by substrate binding. Alignment of the structures shows that a simple hinge motion centered on the conserved residues Phe268 and Thr269 moves the C-terminal domain by about 30° relative to the rest of the molecule. This domain motion positions a conserved aspartate residue located in the C-terminal domain in the active site of the adjacent monomer, which may serve as a general acid/base in the catalytic mechanism.

1. Introduction

Malyl-CoA lyase (MCL; EC 4.1.3.2) catalyzes the reversible aldol cleavage of (2*S*)-4-malyl-CoA to form acetyl-CoA and glyoxylate (Hacking & Quayle, 1974). It is a member of the citrate lyase β-subunit-like family (Finn *et al.*, 2016), which includes citrate lyase (EC 4.1.3.6) and malate synthase (EC 2.3.3.9) (Zarzycki & Kerfeld, 2013). MCL was first isolated from *Methylobacterium extorquens* AM1, where it plays a central role in the *icl*$^-$ serine pathway for formaldehyde assimilation during growth on C_1 compounds (Anthony, 1982). During growth on methanol, *M. extorquens* AM1 derives its energy from the oxidation of methanol by PQQ-dependent methanol dehydrogenase. Formaldehyde is then assimilated *via* the serine hydroxymethyl transferase-catalyzed condensation of 5,10-methylene tetrahydrofolate and glycine. In the serine pathway, MCL provides glyoxylate for the regeneration of glycine. In *M. extorquens* AM1, the gene encoding MCL exists in an operon encoding C_1 metabolism genes and its expression is induced during growth on methanol (Arps *et al.*, 1993; Chistoserdova & Lidstrom, 1992; Fulton *et al.*, 1984).

MCL from *M. extorquens* AM1 has a monomer molecular mass of 34 kDa and thought to exist as a hexamer in solution (Hacking & Quayle, 1974, 1990). MCL requires Mg^{2+} or Co^{2+} for activity and is specific for (2*S*)-4-malyl-CoA for the cleavage reaction. The (2*R*) enantiomer of 4-malyl-CoA is a competitive inhibitor of the cleavage reaction. In the reverse reaction, MCL condenses acetyl-CoA or propionyl-CoA with

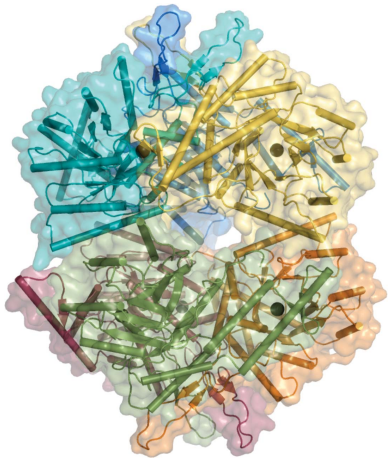

Table 1
Macromolecule-production information.

Source organism	*M. extorquens* (strain DSM 5838/DM4)
DNA source	Synthetic (Genewiz)
Forward primer	N/A
Reverse primer	N/A
Cloning vector	pET-42a(+), Novagen
Expression vector	pET-42a(+), Novagen
Expression host	*E. coli* Arctic Express (DE3), Stratagene
Complete amino-acid sequence of the construct produced	MSFTLIQQATPRLHRSELAVPGSNPTFMEKSAAS-KADVIFLDLEDAVAPDDKEQARKNIIQALNDL-DWGNKTMMIRINGLDTHYMYRDVVDIVEACPR-LDMILIPKVGVPADVYAIDVLTTQIEQAKKRE-KKIGFEVLIETALGMANVEAIATSSKRLEAMS-FGVADYAASTRARSTVIGGVNADYSVLTDKDE-AGNRQTHWQDPWLFAQNRMLVACRAYGLRPID-GPFGDFSDPDGYTSAARRCAALGFEGKWAIHP-SQIDLANEVFTPSEAEVTKARRILEAMEEAAK-AGRGAVSLDGRLIDIASIRMAEALIQKADAMG-GKEHHHHHHHH

glyoxylate to yield (2*S*)-4-malyl-CoA or (2*S*)-4-(β-methyl)-malyl-CoA, respectively. MCLs from *Rhodobacter sphaeroides* and *Chloroflexus aurantiacus* have been shown to cleave β-methylmalyl-CoA and to condense pyruvate and acetyl-CoA to yield citramalyl-CoA (Zarzycki & Kerfeld, 2013; Erb *et al.*, 2010; Herter *et al.*, 2002; Zarzycki *et al.*, 2009).

Our interest in MCL for metabolic engineering lies in its potential as an alternative to pyruvate dehydrogenase as a source of acetyl-CoA. Here, we report the 1.56 Å resolution structure of *M. extorquens* AM1 malyl-CoA lyase (*Mex*MCL) crystallized in the presence of Mg^{2+}. Based on the recently reported MCL structures and its close sequence identity to *R. sphaeroides* MCL (*Rsp*MCL; 57% identity) and *C. aurantiacus* MCL (*Cau*MCL; 30% identity) (Zarzycki & Kerfeld, 2013), we can infer the domain movements that are likely to occur upon the binding of malyl-CoA or acetyl-CoA to *Mex*MCL.

2. Materials and methods

2.1. Macromolecule production

2.1.1. Materials. All chemicals were obtained from Sigma–Aldrich, unless otherwise stated. The oligonucleotide-synthesis and DNA-sequencing reactions were performed by Genewiz Inc. The pET-42a(+) expression vector was purchased from Novagen. Arctic Express (DE3) competent cells were acquired from Stratagene.

2.1.2. Cloning of MCL. The gene encoding malyl-CoA lyase from *M. extorquens* AM1 was synthesized with codons optimized for protein expression in *Escherichia coli* and then subcloned into pET-42a(+) by Genewiz Inc. The cloning sites NdeI and XhoI were used to obtain a clone expressing *Mex*MCL with a His_8 tag at the C-terminus of the protein (*Mex*MCL-His_8; Table 1).

2.1.3. Protein expression and purification. The expression vector encoding *Mex*MCL was transformed into Arctic-Express (DE3) competent cells and plated onto an LB/agar plate containing 50 µg ml^{-1} kanamycin. A single colony was cultured overnight in 25 ml of LB medium containing 50 µg ml^{-1} kanamycin; 4 ml of the culture was then used to inoculate 2 l of the same medium. Cell cultures were grown at 37°C with a rotary shaker until an optical density (600 nm) of 0.6 was reached, after which the temperature was decreased to 16°C and induction was initiated by the addition of isopropyl β-D-1-thiogalactopyranoside (IPTG) to a final concentration of 1.0 m*M*. The culture was then incubated overnight at 16°C. The bacterial cells were pelleted by centrifugation at 7000*g* for 10 min at 4°C. The pellet was washed and resuspended in 20 m*M* sodium phosphate buffer containing 50 m*M* NaCl and 5 m*M* imidazole at pH 7.4 (buffer *A*). 5 µg ml^{-1} DNAse and 0.1 mg ml^{-1} of the protease inhibitor PMSF per gram of cells were also added to the buffer *A* before cell disruption. The resuspended cells were cooled in an ice bath and lysed by sonication (Cole Palmer Sonic Processor). Using an amplitude of 95%, the sonicator was cycled for 2 s on followed by 2 s off for a total of 10 min. The sample was then cooled for 5 min. This sonication cycle was carried out a total of three times. The soluble protein was separated from the cell debris by centrifugation at 12 000*g* for 15 min at 4°C and then loaded onto two 5 ml HisTrap columns connected in tandem and equilibrated with buffer *A*. *Mex*MCL-His_8 was eluted with a linear gradient from 20 to 500 m*M* imidazole over ten column volumes in a buffer consisting of 20 m*M* sodium phosphate, 50 m*M* NaCl pH 7.4 (buffer *B*). Fractions containing *Mex*MCL-His_8 were pooled, concentrated and loaded onto a HiLoad 26/60 Superdex 200 prep-grade gel-filtration column (GE Healthcare) and eluted with 20 m*M* HEPES buffer containing 50 m*M* NaCl at pH 7.2 (buffer *C*). The purity of the protein during the isolation procedure was monitored by SDS–PAGE using Kaleidoscope prestained standards (molecular weight 7.6–216 kDa; Bio-Rad). The protein concentration was estimated from the absorbance at 280 nm using a theoretical extinction coefficient of 32.5 mM^{-1} cm^{-1} (Gill & von Hippel, 1989) calculated using the protein identification and analysis tools on the ExPASy server.

Table 2
Crystallization.

Method	Vapor diffusion, sitting drop
Plate type	96-well, Intelli-Plate; 24-well, VDX
Temperature (K)	298
Protein concentration (mg ml^{-1})	25
Buffer composition of protein solution	10 m*M* HEPES pH 8.0, 20 m*M* NaCl
Composition of reservoir solution	0.1 *M* HEPES pH 7.5, 30%(*w*/*v*) PEG 400, 0.2 *M* $MgCl_2$
Volume and ratio of drop	2.0 µl:2.0 µl
Volume of reservoir (µl)	1000

2.2. Crystallization

Crystals of *Mex*MCL were grown using the sitting-drop vapor-diffusion method in 96-3 Intelli-Plate trays (Art Robbins Instruments; Table 2). Drops consisting of 1 µl of a 1:1 mixture of protein sample (25 mg ml^{-1} in 10 m*M* HEPES pH 8, 20 m*M* NaCl) and reservoir solution were prepared with an Oryx8 liquid-handling robot (Douglas Instruments). Initial crystallization trials consisted of the commercial screens MCSG-1, MCSG-2, MCSG-3 and MCSG-4 (Microlytic).

Table 3
Data collection and processing.

Values in parentheses are for the outer shell.

Diffraction source	Beamline 7-1, SSRL
Wavelength (Å)	1.127092
Temperature (K)	100
Detector	ADSC Quantum 315r
Crystal-to-detector distance (mm)	183.1
Rotation range per image (°)	0.2
Total rotation range (°)	90
Exposure time per image (s)	0.2
Space group	*P*622
a, *b*, *c* (Å)	126.52, 126.52, 103.21
α, β, γ (°)	90, 90, 120
Mosaicity (°)	0.11
Resolution range (Å)	38.47–1.56 (1.59–1.56)
Total No. of reflections	695287 (15465)
No. of unique reflections	62486 (2642)
Completeness (%)	91.1 (79.3)
Multiplicity	11.1 (5.9)
$\langle I/\sigma(I)\rangle$	22.2 (2.7)
$R_{\rm meas}$	0.064 (0.607)
$CC_{1/2}$	0.999 (0.845)
Overall *B* factor from Wilson plot (Å^2)	13.7

Table 4
Structure solution and refinement.

Values in parentheses are for the outer shell.

Resolution range (Å)	38.44–1.56 (1.59–1.56)
σ Cutoff	0†
No. of reflections, working set	59427 (3979)
No. of reflections, test set	3059 (207)
Final $R_{\rm cryst}$	0.103 (0.160)
Final $R_{\rm free}$	0.136 (0.190)
Cruickshank DPI (Å)	0.048
No. of non-H atoms	
Protein	2554
Ion	2
Ligand	16
Water	383
R.m.s. deviations	
Bonds (Å)	0.018
Angles (°)	1.931
Average *B* factors (Å^2)	
Protein	20.2
Ion	15.8
Ligand	47.6
Water	33.5
Ramachandran plot	
Most favored (%)	95.1
Allowed (%)	4.9

† The σ-cutoff value for scaling was not enforced, but structure factors were calculated with the algorithm of French and Wilson as implemented in *TRUNCATE* (French & Wilson, 1978).

Hexagonal prism-shaped crystals of ∼150 µm in size appeared after 3–4 d of incubation at 298 K in a medium consisting of 0.1 *M* HEPES pH 7.5, 30%(*w*/*v*) PPG 400, 0.2 *M* $MgCl_2$ (mother liquor), corresponding to condition No. 30 of the MCSG-1 crystallization suite (Midwest Center for Structural Genomics). Crystals were successfully reproduced in 24-well VDX plates in a sitting-drop setup with micro-bridges (Hampton Research), with 4 µl 1:1 drops and 1 ml reservoir, where polypropylene glycol 400 (PPG 400) was replaced by polyethylene glycol 400 (PEG 400) (Supplementary Fig. S1). Crystals were cryoprotected in the mother liquor diluted by the addition of glycerol to a final concentration of 20%, mounted in nylon loops (Hampton) and flash-cooled in liquid nitrogen.

2.3. Data collection and processing

Diffraction data for *Mex*MCL were collected remotely on beamline 7-1 of the Stanford Synchrotron Radiation Light Source (SSRL) at a wavelength of 1.127 Å using an ADSC Quantum 315r CCD detector (Cohen *et al.*, 2002; Soltis *et al.*, 2008). Reflections were indexed with *iMosflm* (Powell *et al.*, 2013) and integrated with *XDS* (Kabsch, 2010). Scaling was performed with *AIMLESS* (Evans & Murshudov, 2013), including structure-factor calculation with the French and Wilson algorithm implemented in *TRUNCATE* (French & Wilson, 1978) and space-group determination with *POINTLESS* (Evans, 2006). Data-collection and quality statistics are summarized in Table 3.

2.4. Structure solution and refinement

The data were phased by molecular replacement with *Phaser* (McCoy *et al.*, 2007). The structure of MCL from *R. sphaeroides* (PDB entry 4l9z; Zarzycki & Kerfeld, 2013) was used as the phasing model, in which all noncovalently bound ligands, alternate conformers and solvent molecules were removed and a random shift of 0.3 Å was added to the remaining protein-atom coordinates to minimize model bias. Structure refinement was performed with *REFMAC*5 (Murshudov *et al.*, 2011) and the *CCP*4 suite (Winn *et al.*, 2011). Manual building was conducted with *Coot* (Emsley *et al.*, 2010) using $\sigma_{\rm A}$-weighted $2mF_{\rm o} - DF_{\rm c}$ and $mF_{\rm o} - DF_{\rm c}$ Fourier difference maps. Structure validation was performed with *SFCHECK* (Vaguine *et al.*, 1999) and the built-in functions implemented in *Coot*. The model was refined to $R_{\rm cryst}$ and $R_{\rm free}$ values of 0.142 and 0.165, respectively, which were further improved to 0.104 and 0.136, respectively, by tightening the geometry matrix with a factor of 1.6 while refining anisotropic *B* factors for all atoms. In this way, excellent geometry was achieved, with final root-mean-square deviations of 0.018 Å and 1.931° for bond lengths and angles, respectively, and no outlier residues in the Ramachandran plot. Lys127 displayed a ring-shaped density around the side-chain ε-amino group, which was modeled as a PEG fragment in a crown-ether complex around the positively charged Lys127 ε-amino group (Supplementary Fig. S4). Structure-solution and refinement statistics are reported in Table 4. The refined structure has been deposited in the PDB as entry 5ugr. Figures were prepared with *PyMOL* v.1.2 (Schrödinger) and *CorelDraw* X7 (Corel).

3. Results and discussion

The structure of *Mex*MCL was solved by molecular replacement and the model was refined to an $R_{\rm free}$ of 13.6% (Table 4), containing nearly all of the amino acids in the protein (Table 1). There is relatively little variation in the atomic displacement parameter (*B* factor), suggesting a rather rigid

overall structure in the absence of CoA or other substrates. The monomer structure (Fig. 1) is composed of an N-terminal $\alpha_8\beta_8$ TIM-barrel fold (residues 12–164 and 198–267), with an extended 'insertion' domain (residues 165–267) and a primarily α-helical C-terminal domain (residues 268–318). *Mex*MCL, as well as *Rsp*MCL and *Cau*MCL, crystallize as hexamers, despite the different pH values and space groups; it is therefore likely that these enzymes exist as physiological hexamers (Fig. 2). This is also suggested by structural analysis of the structure of *Mex*MCL using the *PISA* server (Krissinel & Henrick, 2007) and by the results of sedimentation-velocity experiments (Hacking & Quayle, 1974).

Mg^{2+}, the active-site metal cofactor, is hexacoordinated in an octahedral geometry by the side-chain carboxylates of Asp45, Glu140 and Asp167 and by three solvent molecules. The coordination distances range from 2.0 to 2.1 Å, which are typical of Mg^{2+} metal-binding sites (Fig. 3*b*, Supplementary Fig. S2). One of the solvent molecules coordinating Mg^{2+} is stabilized by hydrogen-bonding interactions with the conserved Glu44 residue. A second ion was found in the second coordination shell of Mg^{2+} and was modeled as a Cl^- ion, which is an abundant anion in the crystallization medium.

A comparison of *Mex*MCL with the enzymes from *R. sphaeroides* and *C. aurantiacus* shows that they share a similar overall fold, with an r.m.s.d. on C^α positions of 0.9–1.3 Å, in line with their sequence similarities, *i.e.* 57% with *Rsp*MCL and 30% with *Cau*MCL (Supplementary Fig. S3).

The TIM domain with the insertion sequence, residues 12–267, and the α-helical C-terminal domain, residues 269–318, align with C^α r.m.s.d.s of 1.1 and 1.67 Å, respectively. However, as illustrated in Fig. 1, when the Mg^{2+}-bound substrate-free form of *Mex*MCL is compared with the liganded structures of *Rsp*MCL the C-terminal domains differ in their relative orientations by ∼30° on average relative to the aligned TIM-barrel domains. A superposition of the three-dimensional structures shows that a simple hinge motion centered on the conserved residues Phe268 and Thr269 (*Mex*MCL numbering) moves the C-terminal domain relative to the rest of the molecule (Figs. 3*a* and 3*c*). It should be noted that three of the six molecules in the asymmetric unit of *Rsp*MCL (PDB entry 4l9y) did not exhibit any domain motion, and these molecules did not contain discernible density for the ligands. All six molecules in the asymmetric unit of *Rsp*MCL (PDB entry 4l9z) contained the ligands. Therefore, the hinge motion of the C-terminal domain relative to the rest of the molecule appears to be correlated with ligand binding. Using the *DynDom* server (Hayward & Berendsen, 1998) and taking advantage of the six molecules in the asymmetric unit of *Rsp*MCL for the Mg^{2+}–glyoxylate–propionyl-CoA complex and the six molecules for the Mg^{2+}–oxalate–CoA complex, we found the domain shift to be on average an ∼30° shift, resulting in a 70% closure. This may be attributable to the binding of the CoA species in this case with oxalate or glyoxylate.

A closer look at the active-site environment of *Mex*MCL shows that there is a Cl^- ion occupying a pocket adjacent to the active site (Fig. 3*b*). A comparison with the *Rsp*MCL structure in complex with oxalate and CoA (Fig. 3*d*) shows

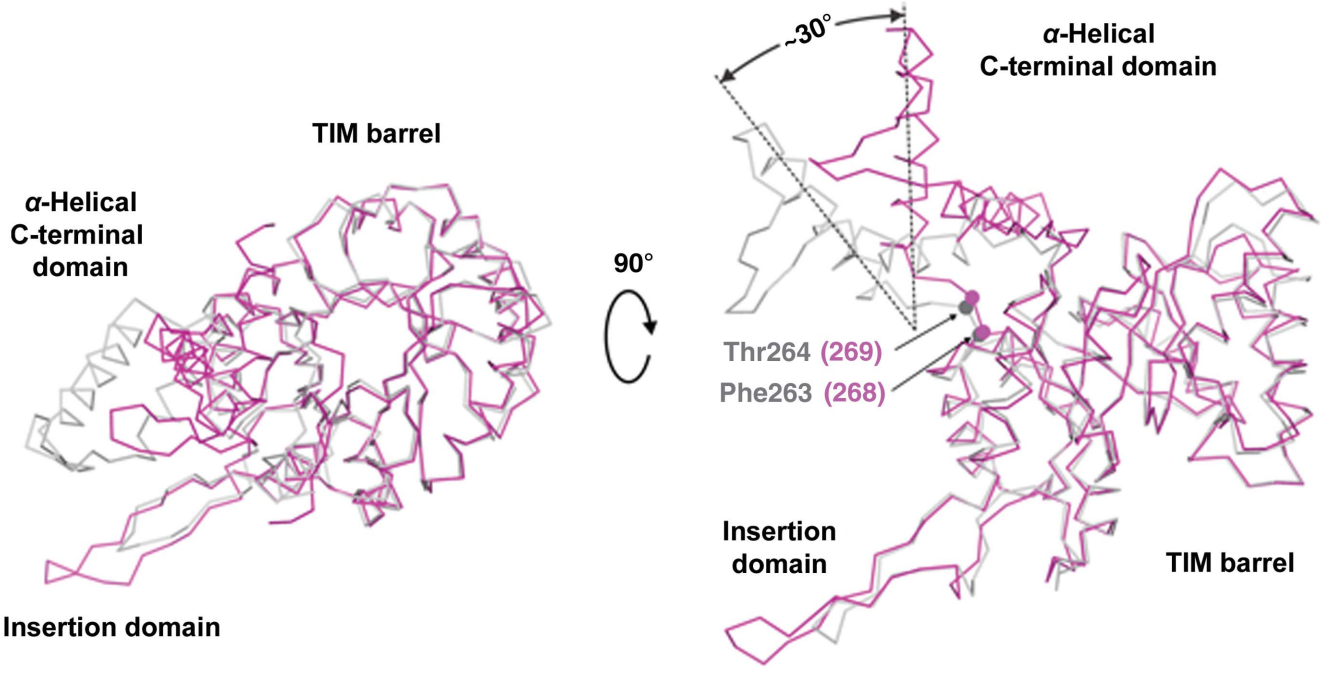

Figure 1
Superposition of backbone traces of the *Mex*MCL–Mg^{2+} monomer (purple) and the *Rsp*MCL–Mg^{2+}–oxalate–CoA monomer (pink). On the left is a view down the center of the TIM barrel. The view on the right illustrates the ∼30° shift of the α-helical C-terminal domain with motion around *Mex*MCL Phe268 and Thr269, corresponding to *Rsp*MCL Phe264 and Thr265. The TIM barrel, insertion domain and C-terminal domain are marked.

that binding of oxalate imparts a minor set of conformational changes, while occupying an equivalent position to the Cl^- ion in *Mex*MCL. A water molecule coordinated to the Mg^{2+} ion is displaced, and the oxalate is doubly coordinated to the Mg^{2+} ion. The direct coordination of the carboxylate of Asp45 is lost, and the side chain of Asp45 swings away and hydrogen-bonds to a water molecule, which in turn coordinates the Mg^{2+} ion (compare Figs. 3*b* and 3*d*). Aside from these rearrangements, there is little change to the active-site topology upon the binding of oxalate. The binding site for oxalate (a glyoxylate analog) is thus mostly pre-formed. Consequently, the 30° domain shift results mostly from the binding of CoA and/or its thioester conjugates, as witnessed for the *Rsp*MCL structure (Zarzycki & Kerfeld, 2013). This domain shift brings the conserved residue Asp299 (*Rsp*MCL)/Asp304 (*Mex*MCL) into the active site of the adjacent monomer (Fig. 3*d*). This residue has been postulated to be involved in the protonation of the CoA–enolate intermediate in the lyase reaction and the deprotonation of acetyl-CoA or propionyl-CoA in the condensation reaction (Zarzycki & Kerfeld, 2013). Despite the substantial phylogenetic differences among microorganisms such as *C. aurantiacus*, *R. sphaeroides* and *M. extorquens*, they share conserved malyl-CoA lyase enzymes, highlighting their essential role in autotrophic carbon assimilation under

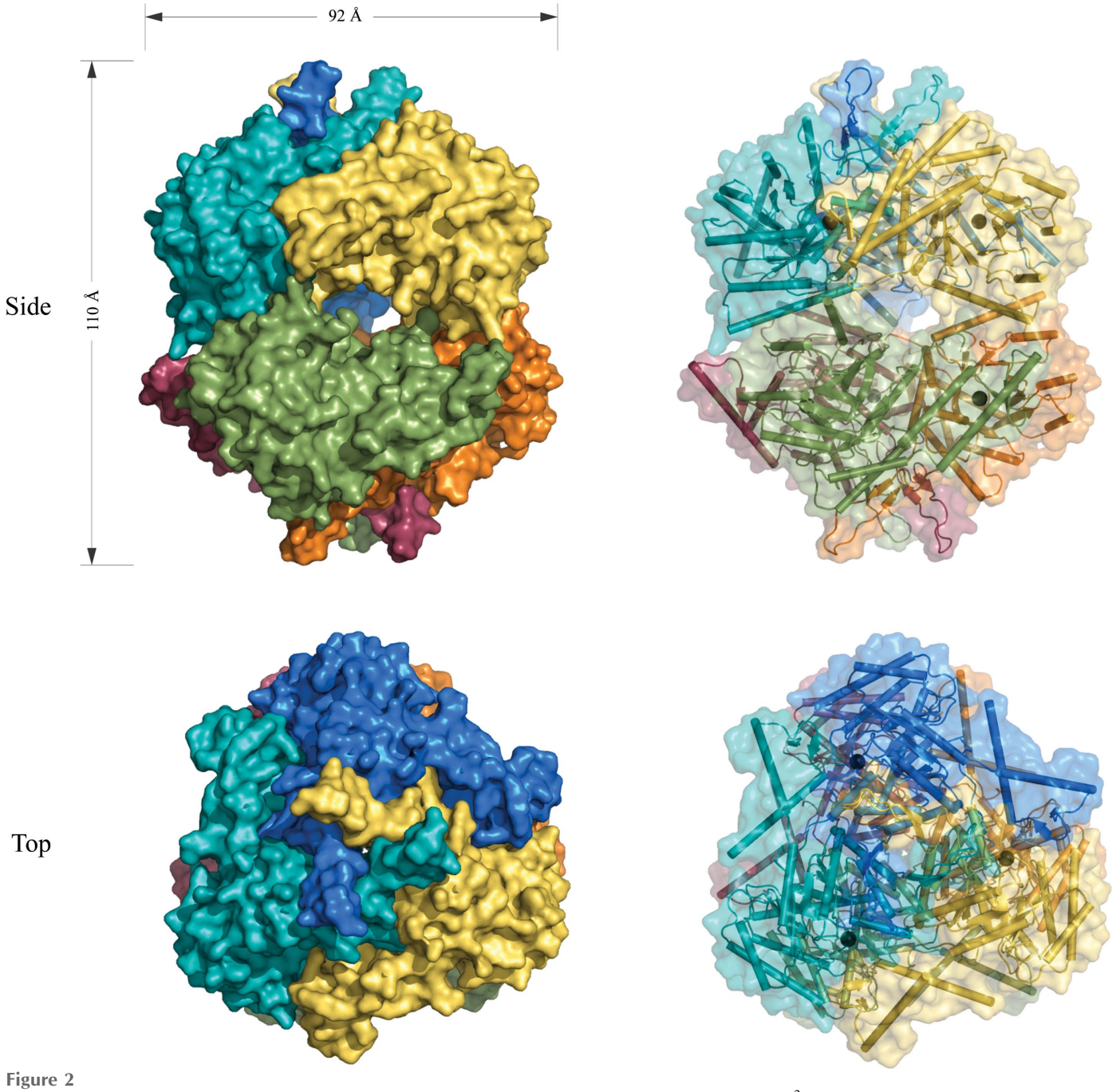

Figure 2
Graphical representation of the quaternary structure of *Mex*MCL (hexameric). Black spheres indicate Mg^{2+}-binding sites.

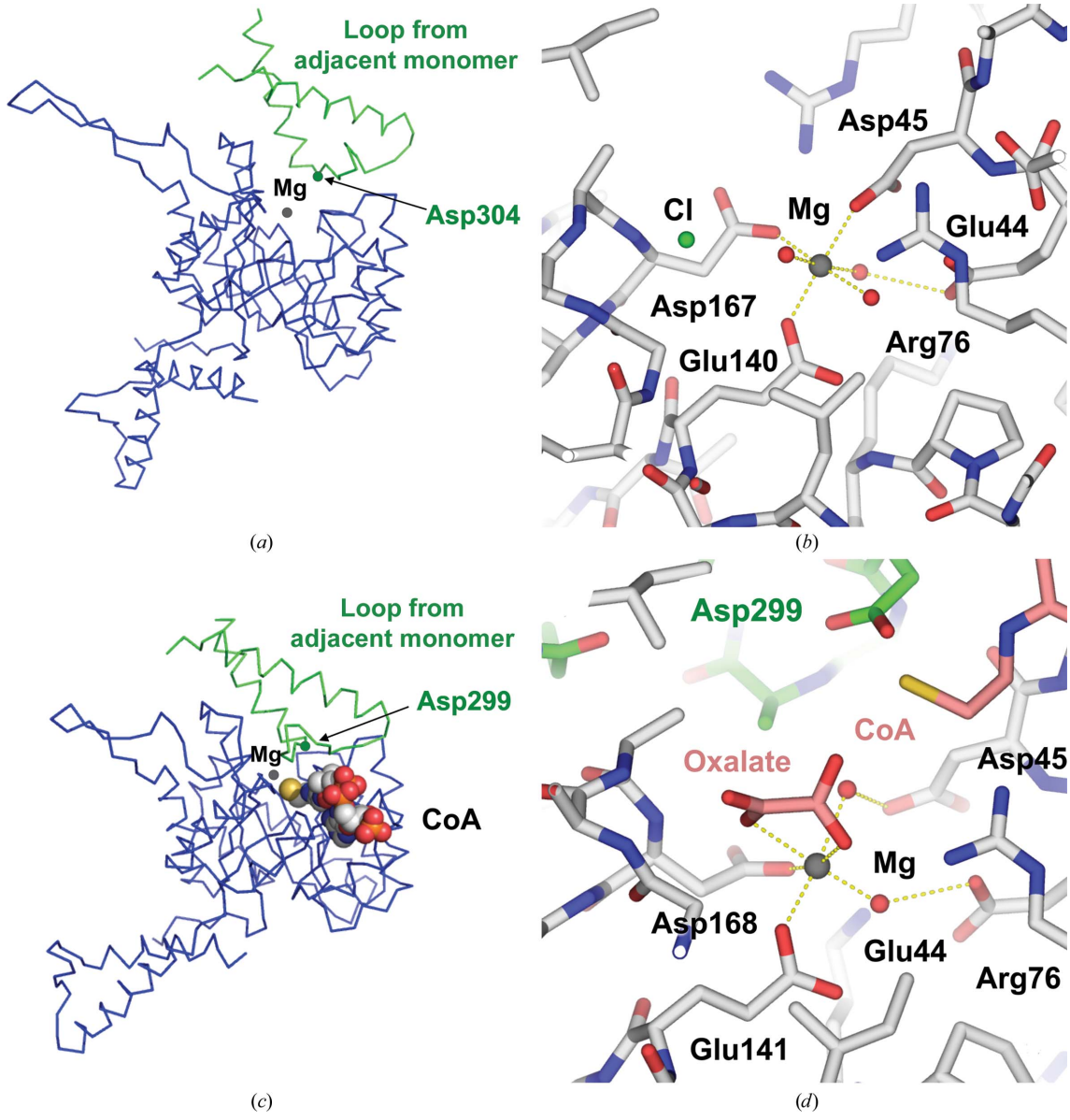

Figure 3
Structural changes upon oxalate and CoA binding. (*a*) A backbone trace of *Mex*MCL (blue), showing the orientation of the adjacent C-terminal domain (green) of the neighboring monomer closest to the active site. The positions of the active-site Mg^{2+} ion and Asp304 (Asp299 in *Rsp*MCL numbering) of the neighboring C-terminal domain are marked. (*b*) Details of the active site of *Mex*MCL–Mg^{2+}, highlighting the conserved amino acids (Asp45, Glu140, Asp167 and Glu44) coordinating the Mg^{2+} ion. (*c*) A backbone trace of *Rsp*MCL–Mg^{2+}–oxalate–CoA (blue), showing the orientation of the adjacent C-terminal domain (green) of the neighboring monomer closest to the active site when bound with oxalate and CoA (space-filling). *Rsp*MCL Asp299 of the adjacent monomer moves close to the bound CoA. (*d*) Details of the active site of *Rsp*MCL–Mg^{2+}–oxalate–CoA, highlighting the conserved amino acids (Asp45, Glu141 and Asp168) coordinating the Mg^{2+} ion. An additional conserved amino acid, Glu44, is involved in hydrogen bonding to a water molecule that coordinates the Mg^{2+} ion. The bound oxalate participates in a bidentate coordination of the Mg^{2+} ion, displacing a water molecule and Cl^{-} ion. The adjacent C-terminal domain shifts towards the active site, bringing the conserved residue Asp299 (green C atoms) into proximity of the bound CoA (pink C atoms).

stress conditions in different species. Further studies are needed to discern the MCL reaction mechanism, allowing new metabolic and enzyme-engineering applications.

4. Related literature

The following references are cited in the Supporting Information for this article: Robert & Gouet (2014).

Acknowledgements

Portions of this research were carried out at the Stanford Synchrotron Radiation Laboratory (SSRL), a national user facility operated by Stanford University on behalf of the US Department of Energy, Office of Basic Energy Sciences. The SSRL Structural Molecular Biology Program is supported by the Department of Energy, Office of Biological and Environmental Research and by the NIH, National Center for

Research Resources, Biomedical Technology Program and the National Institute of General Medical Sciences. We thank Virginia Unkefer for editing of the manuscript. JMG is the recipient of an LANL Director's Postdoctoral Fellowship (grant DOE-LDRD 20120776PRD4).

Funding information

Funding for this research was provided by: Los Alamos National Laboratory (award No. 20130091DR).

References

Anthony, C. (1982). *The Biochemistry of Methylotrophs.* London: Academic Press.
Arps, P. J., Fulton, G. F., Minnich, E. C. & Lidstrom, M. E. (1993). *J. Bacteriol.* **175**, 3776–3783.
Chistoserdova, L. V. & Lidstrom, M. E. (1992). *J. Bacteriol.* **174**, 71–77.
Cohen, A. E., Ellis, P. J., Miller, M. D., Deacon, A. M. & Phizackerley, R. P. (2002). *J. Appl. Cryst.* **35**, 720–726.
Emsley, P., Lohkamp, B., Scott, W. G. & Cowtan, K. (2010). *Acta Cryst.* D**66**, 486–501.
Erb, T. J., Frerichs-Revermann, L., Fuchs, G. & Alber, B. E. (2010). *J. Bacteriol.* **192**, 1249–1258.
Evans, P. (2006). *Acta Cryst.* D**62**, 72–82.
Evans, P. R. & Murshudov, G. N. (2013). *Acta Cryst.* D**69**, 1204–1214.
Finn, R. D., Coggill, P., Eberhardt, R. Y., Eddy, S. R., Mistry, J., Mitchell, A. L., Potter, S. C., Punta, M., Qureshi, M., Sangrador-Vegas, A., Salazar, G. A., Tate, J. & Bateman, A. (2016). *Nucleic Acids Res.* **44**, D279–D285.
French, S. & Wilson, K. (1978). *Acta Cryst.* A**34**, 517–525.
Fulton, G. L., Nunn, D. N. & Lidstrom, M. E. (1984). *J. Bacteriol.* **160**, 718–723.
Gill, S. C. & von Hippel, P. H. (1989). *Anal. Biochem.* **182**, 319–326.
Hacking, A. J. & Quayle, J. R. (1974). *Biochem. J.* **139**, 399–405.
Hacking, A. J. & Quayle, J. R. (1990). *Methods Enzymol.* **188**, 379–386.
Hayward, S. & Berendsen, H. J. (1998). *Proteins*, **30**, 144–154.
Herter, S., Busch, A. & Fuchs, G. (2002). *J. Bacteriol.* **184**, 5999–6006.
Kabsch, W. (2010). *Acta Cryst.* D**66**, 133–144.
Krissinel, E. & Henrick, K. (2007). *J. Mol. Biol.* **372**, 774–797.
McCoy, A. J., Grosse-Kunstleve, R. W., Adams, P. D., Winn, M. D., Storoni, L. C. & Read, R. J. (2007). *J. Appl. Cryst.* **40**, 658–674.
Murshudov, G. N., Skubák, P., Lebedev, A. A., Pannu, N. S., Steiner, R. A., Nicholls, R. A., Winn, M. D., Long, F. & Vagin, A. A. (2011). *Acta Cryst.* D**67**, 355–367.
Powell, H. R., Johnson, O. & Leslie, A. G. W. (2013). *Acta Cryst.* D**69**, 1195–1203.
Robert, X. & Gouet, P. (2014). *Nucleic Acids Res.* **42**, W320–W324.
Soltis, S. M. *et al.* (2008). *Acta Cryst.* D**64**, 1210–1221.
Vaguine, A. A., Richelle, J. & Wodak, S. J. (1999). *Acta Cryst.* D**55**, 191–205.
Winn, M. D., Ballard, C. C., Cowtan, K. D., Dodson, E. J., Emsley, P., Evans, P. R., Keegan, R. M., Krissinel, E. B., Leslie, A. G. & McCoy, A. (2011). *Acta Cryst.* D**67**, 235–242.
Zarzycki, J., Brecht, V., Müller, M. & Fuchs, G. (2009). *Proc. Natl Acad. Sci. USA*, **106**, 21317–21322.
Zarzycki, J. & Kerfeld, C. A. (2013). *BMC Struct. Biol.* **13**, 28.